Impact of Runoff Schemes on Global Flow Discharge: A Comprehensive Analysis Using the Noah-MP and CaMa-Flood Models

Mohamed Hamitouche[1,2,3], Giorgia Fosser[1], Alessandro Anav [2,3], Cenlin He[4], Tzu-Shun Lin [4]

5   [1]University School for Advanced Studies IUSS, Pavia, Italy
[2]Climate Modeling Laboratory ENEA – Italian National Agency for New Technologies, Energy and Sustainable Economic Development. CR Casaccia, Viale Anguillarese 301, 00123, Santa Maria di Galeria (Rome), Italy
[3]ICSC Italian Research Center on High-Performance Computing, Big Data and Quantum Computing, Bologna, Italy
[4]Research Applications Laboratory, NSF National Center for Atmospheric Research, Boulder, Colorado, USA

Correspondence to: Mohamed Hamitouche (mohamed.hamitouche@iusspavia.it)

Abstract. Accurate estimation of flow discharge is crucial for hydrological modelling, water resources planning, and flood prediction. This study examines seven common runoff schemes within the widely-used Noah-MP land surface model and evaluates their performance, using ERA5-Land runoff data as a benchmark for assessing runoff and in-situ streamflow

15   observations for evaluating discharge across the globe. Then, to assess the sensitivity of global river discharge to runoff, we simulate the discharge, using the CaMa-Flood model, across various climatic regions. The results indicated significant variability in the accuracy of the runoff schemes, with model experiments that use TOPMODEL-based runoff schemes, which are based on topography, underestimates runoff across many regions, particularly in the Northern Hemisphere, while experiments using the other runoff schemes (Schaake, BATS, VIC, and XAJ) showed improved performance. Dynamic VIC

20   consistently overestimated runoff globally. Seasonal analysis reveals substantial regional and seasonal variability. ERA5-Land and several Noah-MP schemes successfully replicated general discharge patterns of in-situ observations, with ERA5-Land and Noah-MP Schaake-scheme simulations closely aligning with observed data. The Noah-MP simulations demonstrated robust versatility across various land covers, soil types, basin sizes, and topographies, indicating its broad applicability. Despite overall good performance, significant biases in high-flow extremes highlight the need for continued

25   model improvement or calibration. This study underscores the importance of improving land and hydrological models for accurate water resource management and climate adaptation strategies.

1 Introduction

Accurate estimation of flow discharge, a fundamental component of global hydrological cycle and a critical water flux from land to ocean (Stephens et al., 2020), is crucial for effective hydrological modelling, water resources planning, flood

30   prediction, and sustainable water management practices. It is essential for flood prediction, aiding in alerts, evacuation plans,

and response strategies (Nguyen et al., 2022). Water supply planning relies on it for equitable allocation across domestic, agricultural, and industrial needs, ensuring sustainability. Ecosystem health benefits from maintaining proper water levels in habitats, safeguarding biodiversity and stability. Infrastructure design and maintenance use accurate estimates for resilient structures against varying conditions. Hydropower generation optimisation and cost management depend on it. Water quality

35 management relies on precise estimation to guide monitoring and pollution control (Zhang et al., 2011). In the context of climate change, it is essential for understanding shifting hydrological patterns and for adapting strategies. Therefore, policies and regulations centred on discharge data necessitate accurate estimation for compliance, equitable allocation, and resource distribution.

On the flip side, runoff and groundwater dynamics are among the most influential physical processes for land surface
40 hydrological simulations, as demonstrated by various on-site and regional simulations (Gan et al., 2019; Li et al., 2020a; Zhang et al., 2016a, 2021a, b; Zheng et al., 2019). Past research has acknowledged the intricate interconnection between runoff and flow discharge, highlighting the propagation of uncertainty from runoff to discharge (David et al., 2019). Recognising their pivotal role, runoff schemes serve as vital components of land surface and hydrological models (Sheng et al., 2017). These models represent the processes governing the conversion of precipitation into runoff. This understanding
45 underscores the significant influence that the selection of a particular runoff scheme can have on flow discharge patterns, yielding profound implications for water resources availability and management. Consequently, there is a pressing demand to conduct a comprehensive quantification of the diverse impacts that various runoff schemes can have on flow discharge.

Runoff schemes, each grounded in distinct hydrological theories and assumptions, can exert diverse influences on flow discharge dynamics. These effects can stem from variations in representation of hydrological processes such as surface
50 runoff, subsurface flow, infiltration, root water uptake, groundwater dynamics, and stream-aquifer interactions (Clark et al., 2015). For instance, schemes that emphasise surface runoff may lead to altered flow pathways and the timing of peak flows, impacting downstream water availability. Conversely, schemes incorporating subsurface processes may enhance groundwater recharge, potentially modifying baseflow contributions and seasonal streamflow patterns.

Moreover, the intricate interactions between runoff schemes, climatic conditions, land cover types, and soil properties,
55 further accentuate their potential impacts on flow discharge (Zipper et al., 2018). Different runoff schemes may exhibit varying sensitivities to climatic variability, resulting in disparate responses to changing precipitation patterns, temperature shifts, and extreme events. Two mechanisms, saturation excess and infiltration excess, jointly contribute to the generation of runoff (Yang et al., 2015). Runoff schemes based on the saturated excess assumption are valid in humid and pervious areas; however, this assumption has limitations in dry and impervious areas where overland flow dominates due to excess
60 infiltration (Ren-Jun, 1992). This underscores the importance of scrutinising runoff scheme behaviour under diverse climate conditions to unravel the complexities of their effects on flow discharge.

Despite prior research has contributed valuable insights into runoff scheme impacts on flow discharge, limitations still persist. Many studies have focused on individual runoff schemes (e.g.: Li et al., 2022) and confined their investigations to specific hydroclimatic contexts (e.g.: Hagemann and Stacke, 2023; Liang et al., 2019) or catchments (e.g.: Rummler et al.,

65 2022; Zheng et al., 2017) that overlook potential interactions and synergies of the diverse runoff schemes when operating globally. A singular focus can limit insights into how runoff schemes collectively shape flow discharge dynamics. Additionally, the generalisation and extrapolation of findings to broader global contexts can be challenging due to geographical and climatic variability, differences in hydrological regimes, land cover, soil types, and other factors.

Given the above-mentioned limitations, this paper aims to elucidate, at global scale, the impact of different runoff schemes

70 on river discharge estimation. To that purpose, we firstly evaluate the performances of seven distinct runoff schemes within the Noah-MP Land Surface Model (LSM), then we simulate flow discharge with the CaMa-Flood River routing model to assess how different runoff schemes affect flow discharge magnitude and dynamics. Our study transcends the boundaries of individual schemes and specific regions, highlighting the need for a holistic assessment that contributes to improved hydrological modelling and management practices.

75 **2 Materials and methods**

2.1 Noah-MP Land Surface Model

In this study, the Noah-MP LSM was applied to simulate global-scale runoff. The Noah-MP LSM is a spatially distributed 1-D model specifically designed to address the vertical routing of surface and subsurface water flow in response to atmospheric forcing, all within individual grid cells. This versatile model incorporates four soil layers, extending to a

80 maximum depth of 2 metres, each with default thicknesses of 0.1 metres, 0.3 metres, 0.6 metres, and 1 metre. It solves Richard's equation to compute the dynamics of soil water content (Chen et al., 1996). In addition to soil water dynamics, Noah-MP computes various surface energy flux components, accounts for gravitational drainage at the lowest soil layer, and handles the partitioning of surface water into infiltration and surface runoff. These computations are facilitated through a range of parameterisation approaches (for detailed information, refer to (He et al., 2023b)).

85 Noah-MP is designed to operate in both uncoupled and coupled modes, seamlessly integrating with atmospheric and/or hydrological models at sub-daily time scales and high spatial resolutions, including point-scale, regional and global simulations. This versatility enables its use in a variety of hydrological, weather, and climate models, offering adaptability across a wide range of spatial and temporal scales while ensuring proper integration in both time and space (He et al., 2023a).

90 Moreover, Noah-MP offers a multi-parameterisation framework that encompasses over 4608 combinations of more than 10 physical processes (Niu et al., 2011) that govern interactions at the land-atmosphere interface. These processes include modules for vegetation dynamics, soil moisture, snowpack accumulation and melt, energy balance, and more. The incorporation of multiple physics-based processes within Noah-MP allows for a comprehensive representation of real-world conditions and facilitates ensemble experiments with the multi-physics model for uncertainty assessment and testing

95 competing hypotheses (Li et al., 2020b; Zhang et al., 2016b).

2.1.1 Noah-MP Parametrisation and Runoff Schemes Overview

The community Noah-Multi parameterisation Land Surface Model (Noah-MP LSM) (Niu et al., 2011; Yang et al., 2011) evolved from the Noah LSM (Chen et al., 1996, 1997; Chen and Dudhia, 2001; Ek et al., 2003), incorporating enhanced physical representations and treatments for dynamic vegetation, canopy interactions, radiative transfer, multi-layer snowpack

100   physics, and soil-hydrological processes. In this study, the last modernised version of Noah-MP (v5.0) with enhanced modularity, interoperability and applicability (He et al., 2023a) was utilised.

As our main focus is on runoff, this study was conducted using the default parametrisation scheme combination outlined in the Noah-MP v5.0 public release code, in uncoupled mode. The main default options include: the Noah-type (Ek et al., 2003) for soil moisture factor, stomatal resistance and evapotranspiration; Monin–Obukhov (M–O) Similarity Theory (MOST)

105   (Monin and Obukhov, 1954) for surface layer exchange coefficient, canopy gaps calculated from the vegetated fraction (gap = 1-VegFrac) (Dickinson, 1983; SELLERS, 1985) and for canopy radiation transfer; the Ball–Berry scheme (Ball et al., 1987; Bonan, 1996) for canopy stomate resistance; Sakaguchi and Zeng's scheme (Sakaguchi and Zeng, 2009) for ground resistance to evaporation/sublimation; the Canadian land surface scheme (CLASS) type (Verseghy, 1991) for ground snow surface albedo, hydraulic properties calculated from total soil water and ice (Niu and Yang, 2006) for frozen soil

110   permeability; the general form of the freezing-point depression equation (Niu and Yang, 2006) for soil supercooled liquid water; and the dynamic vegetation model (Dickinson et al., 1998) turned off but using maximum vegetation fraction and a look-up table for leaf area index.

In this study, we conducted seven simulations with different runoff and groundwater schemes. Each experiment (henceforth EXP) was numbered according to the Noah-MP runoff options as follows:

115   1) TOPMODEL with groundwater (Niu et al., 2007),

2) TOPMODEL with an equilibrium water table (Niu et al., 2005),

3) Original Noah free drainage or Schaake's runoff (Schaake et al., 1996),

4) BATS surface and subsurface runoff (Yang and Dickinson, 1996),

6) Variable Infiltration Capacity (VIC) Model surface runoff scheme (Liang et al., 1994),

120   7) Xinanjiang Infiltration and surface runoff scheme (XAJ, (Jayawardena and Zhou, 2000)),

8) Dynamic VIC surface runoff scheme (Liang and Xie, 2003).

The Miguez-Macho&Fan groundwater scheme ((Fan et al., 2007; Miguez-Macho et al., 2007); Noah-MP runoff option 5) was not included in this analysis due to unavailable global riverbed data and other essential inputs.

Infiltration excess and saturation excess runoff generation processes are the key factors leading to the difference among the

125   selected options. This distinction has a direct impact on the velocity of surface runoff and bottom drainage fluxes, leading to the removal of water mass and shifts in liquid soil water content (Chang et al., 2020).

The TOPMODEL with groundwater approach (EXP1) utilises a simplified groundwater modelling method outlined by (Niu et al., 2007). In this method, vertical recharge to an unconfined aquifer is estimated through a parameterisation of Darcy's

Law. Groundwater storage calculations are then employed to determine the grid-scale water table depth (dwt), which is

130   subsequently converted into the saturated surface fractional area (fsat), given as:

Equation 1

$$fsat = fsat_{max} \times e^{-0.5 \times F \times dwt}$$

where F is the runoff decay factor, and $fsat_{max}$ is the maximum saturated fraction of soil surface (assigned a fixed, unitless

value of 0.38). Surface runoff is calculated using a saturation excess runoff generation process, where fsat is multiplied by

135   the precipitation that falls on the soil surface. Subsurface runoff is assumed to be proportional to exp[-F(dwt)].

TOPMODEL with equilibrium runoff (EXP2) calculations are similar to the previous scheme, with the key difference being

that dwt is determined using an equilibrium water table calculation rather than a dynamic groundwater balance (Niu et al.,

2005, 2011).

Unlike TOPMODEL-based schemes, the Schaake and BATS parameterisations do not account for water table dynamics, but

140   use a gravitational free-drainage baseflow approach as a bottom boundary condition. These two approaches differ in their

treatment of surface runoff. The Schaake approach (EXP3) employs the infiltration excess surface runoff method described

by (Schaake et al., 1996), which is based on an adaptation of the Soil Conservation Service curve number method. In this

approach, the surface runoff prediction is notably sensitive to the Noah-MP parameter REFKDT (Niu and Yang, 2011),

which controls the influence of pre-storm surface soil moisture conditions and is linearly related to the Kdt parameter

145   described by (Schaake et al., 1996). The BATS physics scheme (EXP4), following (Yang and Dickinson, 1996),

parameterises the fraction of incident precipitation converted into runoff as the fourth power of the degree of saturation in

the top 2 metres of the soil column. The gravitational drainage is parametrised in Schaake as the product of the soil drainage

slope index (S_{drain}) and the soil hydraulic conductivity (K_{hyd}), while in BATS as $(1 - F_{frz,max})K_{hyd}$, where $F_{frz,max}$ is the

maximum soil impermeability fraction throughout the soil column.

150   The VIC scheme (EXP6) calculates the saturation excess surface runoff in surface soil layers (two first layers) based on a

variable infiltration capacity function (i) given by:

Equation 2

$$i = i_{max} \times (1 - (1 - A)^{1/b})$$

where A is the fraction of saturated soil in a grid, b is a curve shape parameter.

155   The surface runoff (R_s) estimated by VIC runoff scheme is given as follows:

If the sum of the infiltration capacity (i) and the effective precipitation (P_e) is higher than the maximum infiltration capacity

(i_{max}), then:

Equation 3

$$R_s = P_e - W_{max} + W$$

160   otherwise:

Equation 4

$$R_s = P_e - W_{max} + W + W_{max} \times \left[1 - \frac{i + P_e}{i_{max}}\right]^{(1+b)}$$

with W being the current tension water storage in surface soil layers (layers 1 and 2), and W_{max} the maximum tension water storage in surface soil layers (layers 1 and 2). In impervious surfaces, the surface runoff (R_s) is given as the effective precipitation (P_e).

165

The XAJ infiltration and surface runoff scheme (EXP7) introduces a distinctive approach to hydrological modelling. It addresses the saturation excess runoff generation by incorporating the concept of variable contributing area and using a double parabolic curve to represent the spatial distribution of tension water capacity (maximum soil water deficit, i.e., the difference between field capacity and wilting point), which is considered the essence of the XAJ model (Fang et al., 2017).

170

In the selected Noah-MP version, the runoff generation process within the XinAnJiang scheme acts on the two first soil layers, resulting in the separation of runoff into two components: surface and subsurface runoff, distinguishing between impervious and pervious surfaces (He et al., 2023b). Surface runoff generated from impervious area (R_{im}) is determined by the product of the fraction of imperviousness due to frozen soil (A_{im}) and the effective precipitation (P) (i.e., mean water input on the soil surface). Surface runoff from permeable soil (R_s) is given by equation 5:

175 **Equation 5**

$$R_s = R \times \left(1 - \left(1 - \frac{S}{S_{max}}\right)^{E_x}\right)$$

where R is runoff filled from tension water areas, and expressed as:

Equation 6

$$R = \begin{cases} P_i \times \left[(0.5 - a)^{1-b} \times \left(\frac{W}{W_{max}}\right)^b\right], if\ 0 \le \frac{W}{W_{max}} \le 0.5 - a \\ P_i \times \left[1 - (0.5 + a)^{1-b} \times \left(1 - \frac{W}{W_{max}}\right)^b\right], 0.5 - a < \frac{W}{W_{max}} \le 1 \end{cases}$$

180

with P_i being the fraction of effective precipitation falling on pervious area ($1-A_{im}$). W and W_{max} are respectively the current and maximum tension water storage. S and S_{max} are respectively the current and maximum free water storage. E_x, a and b are shape parameters.

(Liang and Xie, 2001, 2003) extended the VIC model to include the infiltration excess runoff generation process (EXP8). The new parametrisation (Dynamic VIC) dynamically represents both Hortonian and Dunnian runoff generation processes

185

by considering effects of sub-grid spatial heterogeneity of soil properties. The saturation excess runoff (R_{se}) is calculated for the saturated area fraction (A_s) following the concept used in VIC, while the infiltration excess runoff (R_{ie}) is computed for $1-A_s$ area fraction as:

Equation 7

$$R_{ie} = \begin{cases} P - R_{se} - f_{mm} \times \Delta t \times \left[1 - \left(1 - \frac{P - R_{se}}{f_m \times \Delta t}\right)^{b+1}\right], if \; \frac{P - R_{se}}{f_m \times \Delta t} \leq 1 \\ P - R_{se} - f_{mm} \times \Delta t \; , otherwise \end{cases}$$

190   where P is the amount of precipitation over a time step Δt, f_{mm} is the average potential infiltration rate over the 1-A_s area, estimated based on the Philip infiltration scheme (Liang and Xie, 2003) and b is a shape parameter.

The subsurface runoff in VIC, Dynamic VIC and XAJ models is drainage-dependent, and calculated as per Schaake scheme.

2.1.2 Input data

ERA5-Land (Muñoz-Sabater et al., 2021), at 0.1-degree resolution, represents the inaugural operational land product in the

195   European reanalysis (ERA) series. It was derived from high-resolution global numerical simulations conducted by the European Centre for Medium-Range Weather Forecasts (ECMWF). These simulations were driven by downscaled meteorological data sourced from the ERA5 climate reanalysis, which includes adjustments for elevation to enhance the accuracy of near-surface thermodynamic conditions. As a result, ERA5-Land offers a consistent depiction of water and energy cycles across the Earth's land surface (Li et al., 2022).

200   In this study, meteorological variables, including 10m wind speed, 2m air temperature, air humidity, surface pressure, longwave and shortwave downward radiation, and total precipitation, were extracted from the ERA5-Land hourly dataset. Subsequently, these variables were interpolated to a spatial resolution of 0.2° to provide forcing data for the Noah-MP LSM. The soil water content simulations were performed over four distinct soil layers with depths corresponding to ECMWF model specifications: 0-7 cm, 7-28 cm, 28-100 cm, and 100-289 cm.

205   Land cover data was defined using the Modified International Geosphere-Biosphere Programme (IGBP) Moderate Resolution Imaging Spectroradiometer (MODIS) 20-category vegetation dataset, which covers the entire globe with 500m (15 seconds) grid intervals, while soil types were mainly determined by the State Soil Geographic (STATSGO)–FAO soil texture data (Miller and White, 1998).

Prior to conducting runoff evaluation simulations, a 15-year spin-up of the Noah-MP LSM was performed for each model

210   runoff experiment. This involved repeating the 1980-1984 interval three times to reach model stability and enhance accuracy in simulating runoff and related hydrological processes. Following the spin-up phase, model simulations forced by hourly ERA5-Land data were carried out for the period 1985-2023.

2.2 CaMa-Flood River Routing Model

As Noah-MP LSM does not account for horizontal water exchanges, it necessitates supplementation with lateral flow

215   algorithms to achieve accurate simulations of the river discharge. We used the Catchment-based Macro-scale Floodplain model, CaMa-Flood (Yamazaki et al., 2011) due to its ability to simulate global temporal variations and discharge peaks.

CaMa-Flood was proved to realistically simulate river water levels and the hydrodynamics of floodplain inundation (Hirabayashi et al., 2013).

Functioning as a global-scale distributed river model, CaMa-Flood relies on runoff input from a land surface model to
220 simulate water storage and river discharge across a predefined river network map, available at different spatial resolutions: 0.25, 0.1, 0.0833, 0.05 and 0.0166 degree. The model discretises river basins into unit catchments, each delineated by sub-grid river and floodplain topography parameters, providing a nuanced representation of floodplain inundation at a sub-grid scale (Yamazaki et al., 2014). River discharge is calculated using the local inertial equation, accounting for the backwater effect and ensuring a more accurate portrayal of river dynamics (Bates et al., 2010; Yamazaki et al., 2013).

225 In its calculations, CaMa-Flood employs the Manning's friction coefficient for main river channels, set at 0.03. The model dynamically adjusts the calculation time step to meet the Courant-Friedrichs-Lewy condition, ensuring computational stability (Bates et al., 2010; Yamazaki et al., 2013). Additionally, a channel bifurcation flow scheme enhances the model's capability to simulate intricate flow dynamics, particularly in mega deltas. This scheme automatically incorporates bifurcation channels into the global river network map, extracting information from the HydroSHEDS flow direction map
230 and the SRTM3 DEM (Yamazaki et al., 2014).

In this study, the CaMa-Flood model at 0.0833 degree spatial resolution was used. To ensure model stability, CaMa-Flood underwent a dedicated spin-up phase, synchronised with the third iteration of the Noah-MP spin-up, spanning a single 5-year interval from 1980 to 1984. Subsequently, daily runoff data simulated by the seven Noah-MP experiments were interpolated to match the resolution of the CaMa-Flood model, as in the spin-up phase, and used to drive river discharge simulations
235 spanning from 1985 to 2023.

Both Noah-MP and CaMa-Flood models were set up over a global domain covering the land areas between 180°W to 180°E and 60°S to 90°N.

Additionally, ERA5-Land daily runoff was also used to simulate the daily river discharge. This assessment followed a similar procedure, including data interpolation, with a 5-year spin-up period from 1980 to 1984, after which CaMa-Flood
240 discharge simulations were conducted from 1985 to 2023.

2.3 Model Evaluation

Due to the absence of direct runoff observations, ERA5-Land runoff data was utilised as a benchmark for evaluating the Noah-MP simulated runoff. The ERA5-Land runoff is generated using the Tiled ECMWF Scheme for Surface Exchanges over Land incorporating land surface hydrology (H-TESSEL). It represents the total water volume accumulated over the
245 forecast period, divided into surface and subsurface components (Liu et al., 2024). Surface runoff is generated when the maximum infiltration rate is exceeded, as described by the Arno scheme (DÜMENIL and TODINI, 1992), while subsurface water fluxes are governed by Darcy's law, assuming free drainage at the bottom boundary condition (Balsamo et al., 2009; Wipfler et al., 2011).

To quantify the performance of the different runoff schemes, the mean annual runoff bias was analysed, calculated as:

250 **Equation 8**

$$Bias\ (\%) = 100 \times \frac{EXP - ERA5\text{-}Land}{ERA5\text{-}Land}$$

where EXP represents the runoff values for each Noah-MP runoff scheme. To avoid incorrect values due to scarce or null runoff or very high bias resulting from low ERA5-Land runoff values, total-annual ERA5-Land runoff values below 5 mm/yr were masked. This mask was then applied to the corresponding values in all experimental datasets, ensuring

255 consistency with the ERA5-Land.

For the evaluation of the impact of the different runoff schemes on discharge simulated by CaMa-Flood, the model outputs were compared with observed discharge data obtained from the Global Runoff Data Centre (GRDC) and the simulated runoff. The evaluation began with visualizing the temporal dynamics of runoff and discharge through mean seasonal cycle plots. Next, we analysed the runoff bias as calculated using Eq. (8) and compared it with the corresponding discharge bias.

260 Finally, a comprehensive assessment of the model performance for each runoff scheme in terms of daily discharge was conducted using several statistical metrics, including the correlation coefficient (R), standard deviation (SD), mean absolute error (MAE), root mean squared error (RMSE), and the Kling-Gupta Efficiency (KGE). The KGE metric (Gupta et al., 2009) is an aggregated measure of the agreement in timing, magnitude, and variability between simulations and observations. It ranges from $-\infty$ to 1, this latter representing the perfect score. The Taylor diagram (Taylor, 2001), which allows simultaneous

265 evaluation of the temporal correlation and standard deviations, was also used to visually summarise the performance over different climatic regions.

The comparative analysis was conducted over 43 global river basins, where discharge observations are available, spanning four climatic zones classified according to the Köppen climate classification (Kottek et al., 2006), which are: cold, warm temperate, equatorial, and arid regions (Fig. 1). The drainage area of the selected basins, based on the discharge gauge

270 stations, ranges from 16,920 km² for the smallest to 4,671,462 km² for the largest. This ensures that the evaluation of both Noah-MP and CaMa-Flood simulations accounts for a wide range of hydrological and climatic conditions, enhancing the robustness and generalisability of the findings. Sandy loam, sandy clay loam, loam, silt loam, clay loam, and clay are the most dominant soil textures, with loam dominating almost 50% of the basins. In terms of land cover, 40% of the basins are dominated by forests, while the others are primarily covered by shrublands, savannas, grasslands, croplands, barren or

275 sparsely vegetated areas, and wooded tundra. The maximum mean slope is lower than 5%, with the maximum slope reaching 27% (Table S1 in the Supplement).
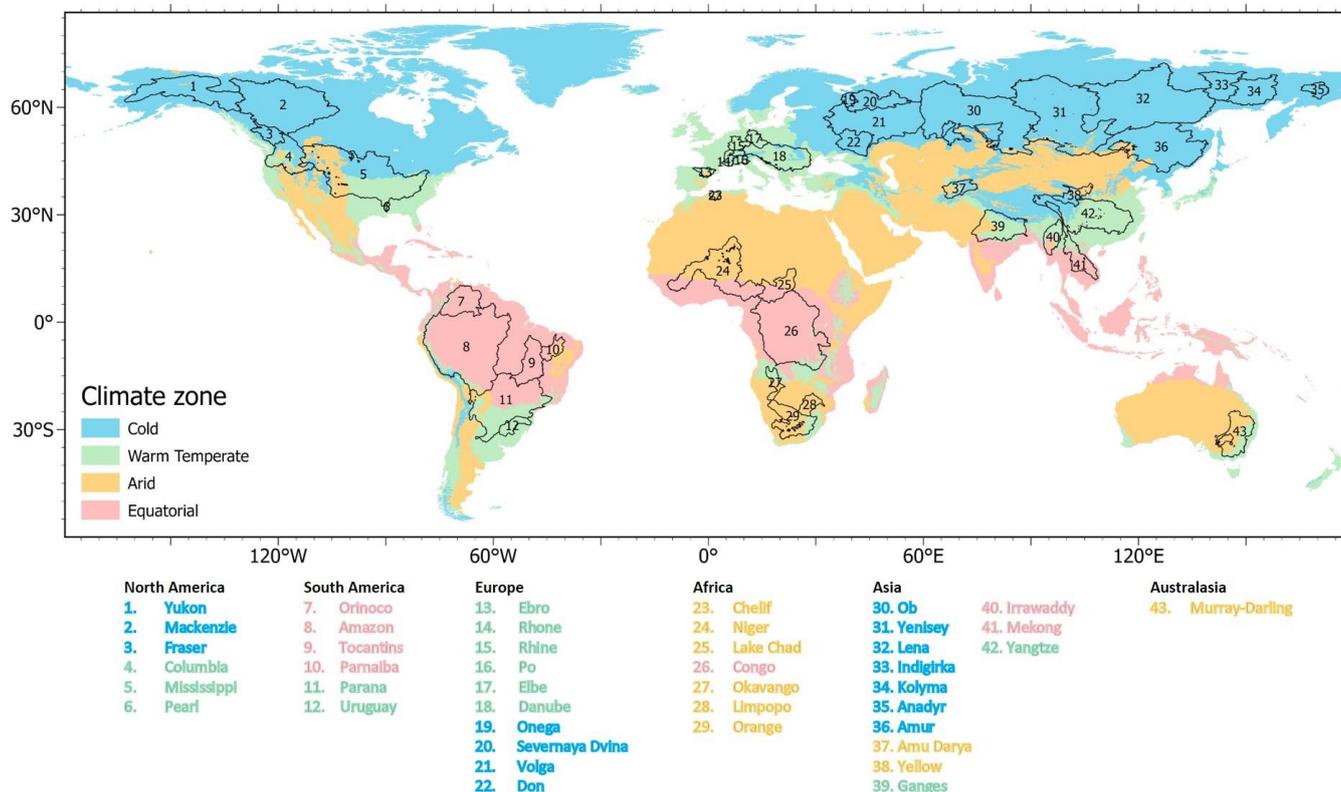
Figure 1: Geographical locations and names of global river basins used in this study, over four climate zones based on The Köppen-Geiger climate classification world map (Kottek et al., 2006)**. The names of the basins are color-coded based on their respective climate zones (Cold, Warm Temperate, Arid, Equatorial). Basins spanning multiple climate zones are assigned to the zone covering the largest area.**

3 Results and discussion

3.1 Runoff Bias

Figure 2 illustrates the spatial pattern of the annual mean (1985-2003) runoff biases of various Noah-MP runoff schemes compared to ERA5-Land runoff data, expressed as percentages. The biases were calculated as in Eq. (8), where positive values indicate overestimation and negative values indicate underestimation of runoff by the Noah-MP experiments relative to ERA5-Land.

In addition, the ERA5-Land runoff map serves as reference, showing the total annual runoff in mm per year. It clearly distinguishes dry areas with runoff of less than around 140 mm per year, mostly corresponding to arid regions, from humid and very humid areas. In equatorial regions, annual runoff can exceed 1000 mm, as seen in the Amazon Basin and parts of south-eastern Asia.
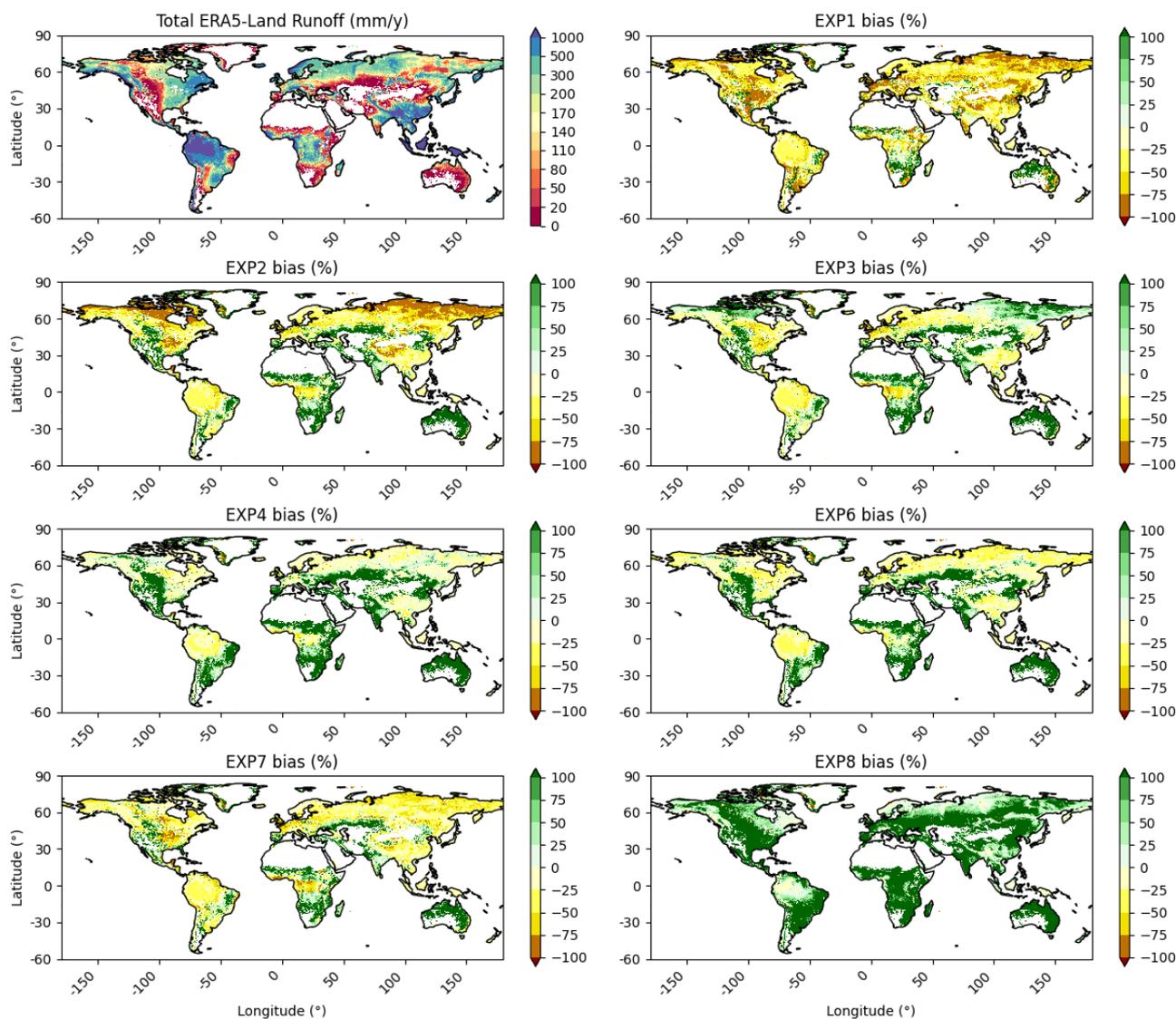
Figure 2: Multi-year mean (1985-2023) annual runoff bias (%) of Noah-MP runoff schemes driven by ERA5-Land climate forcing compared to ERA5-Land runoff data.

295 Across the different experiments, the biases in runoff exhibit substantial spatial variability. In particular, EXP1 generally underestimates runoff compared to ERA5-Land in almost every region, except in central and South Africa, and some limited areas in Eastern South America and Western Australasia. This underestimation is particularly significant in the Northern Hemisphere, especially in cold and warm temperate regions, where the bias often exceeds 50%, reaching up to 100%. This corresponds to a runoff deficit of 100 to 400 mm per year, indicating that EXP1 struggles considerably with capturing runoff

300 dynamics in these areas.

EXP2 exhibits a more balanced bias distribution: while negative biases are still present in the Northern Hemisphere, particularly in Canada and northern Asia, the magnitude is reduced compared to EXP1. There are also slightly more areas with positive bias, mostly less than 50 mm/year, in Africa, Australia, and North and Eastern South America, while negative biases, exceeding 300 mm/yr, are observed in the Amazon basin and Southeast Asia.

305 EXP3 demonstrates reduced biases overall compared to EXP1 and EXP2. In the Southern Hemisphere, its performance is close to EXP2. In the Northern Hemisphere, positive biases, lower than 100% and less than 100 mm/yr, are observed in polar and cold regions. Negative biases are still present but are less intense. This suggests an improved handling of runoff dynamics in these regions.

EXP4 exhibits a similar pattern of bias to EXP3, with a generally lower magnitude of bias compared to the earlier

310 experiments. However, there are still regions with significant positive bias reaching up to around 500 mm/yr, particularly in the equatorial and subequatorial zones.

EXP6 shows a mix of positive and negative biases, but with a generally lower magnitude compared to the earlier experiments. Negative biases, mostly lower than 50%, are particularly evident in the Northern Hemisphere, especially in cold and warm temperate regions with less than 100 mm/yr, and could reach around 200 mm/yr in equatorial regions like the

315 Amazon River basin and parts of Central Asia. Positive biases are also observed in the equatorial and subequatorial zones, ranging from around 50 to 200 mm/yr. However, the extent and intensity of these biases are reduced compared to EXP1 and EXP2, suggesting an improved performance in handling runoff, though not as well as EXP3 and EXP4 in some regions.

EXP7 displays a similar pattern to EXP6, with reduced biases compared to EXP1 and EXP2. Negative biases dominate in the Northern Hemisphere, particularly in high-latitude and warm temperate regions. Positive biases are less widespread but

320 are still present in some equatorial and subequatorial regions, including parts of South America and Africa, Central Asia and Australasia. The overall bias magnitudes are lower than those observed in EXP1 and EXP2, indicating a better performance, though still showing room for improvement in specific regions.

EXP8 displays the most pronounced positive biases (>100%) across nearly all regions. This indicates a substantial overestimation of runoff by this scheme on a global scale, with biases up to around 300 mm in cold regions and up to around

325 500 mm in the other basins. In Dynamic VIC (EXP8), the saturation excess runoff is conceptualised similarly to VIC (EXP6), which performs relatively well compared to ERA5-Land runoff. This suggests that the overestimation is primarily due to the parameterization of the infiltration-excess runoff within Dynamic VIC. With the Dynamic VIC scheme, Noah-MP uses three infiltration measurement methods: Philip (Philip, 1987), Green-Ampt (Heber Green and Ampt, 1911), and Smith-Parlange (Smith and Parlange, 1978) infiltration schemes, with the Philip scheme being used in this study. Improving runoff

330 simulation performance with the Dynamic VIC scheme could be achieved by selecting the most appropriate infiltration scheme and optimising its parameterization.

In summary, the progression from EXP1 through EXP7 shows a trend of decreasing bias magnitudes and improved performance in simulating runoff dynamics. While EXP1 and EXP2 exhibit significant underestimation in many regions, particularly in the Northern Hemisphere, the other experiments like EXP3, EXP4, EXP6, and EXP7 demonstrate

335 progressively better performance with reduced biases. Nonetheless, challenges remain, particularly in accurately capturing runoff in the equatorial and subequatorial areas, as well as in certain high-latitude regions. This analysis underscores the need for ongoing model refinement and calibration to enhance the predictive accuracy of runoff simulations across diverse climatic regions.

3.2 Seasonal Cycle of Runoff and River Discharge

340 The seasonal cycle of both runoff and discharge, as simulated by the Noah-MP experiments and the CaMa-Flood model, reveals significant variability across different climatic zones, highlighting the diverse hydrological processes within each region (Fig. 3). The inclusion of discharge data beneath each corresponding runoff plot emphasizes the connection between these two variables and underscores the crucial role of runoff in shaping the discharge patterns observed in various basins.
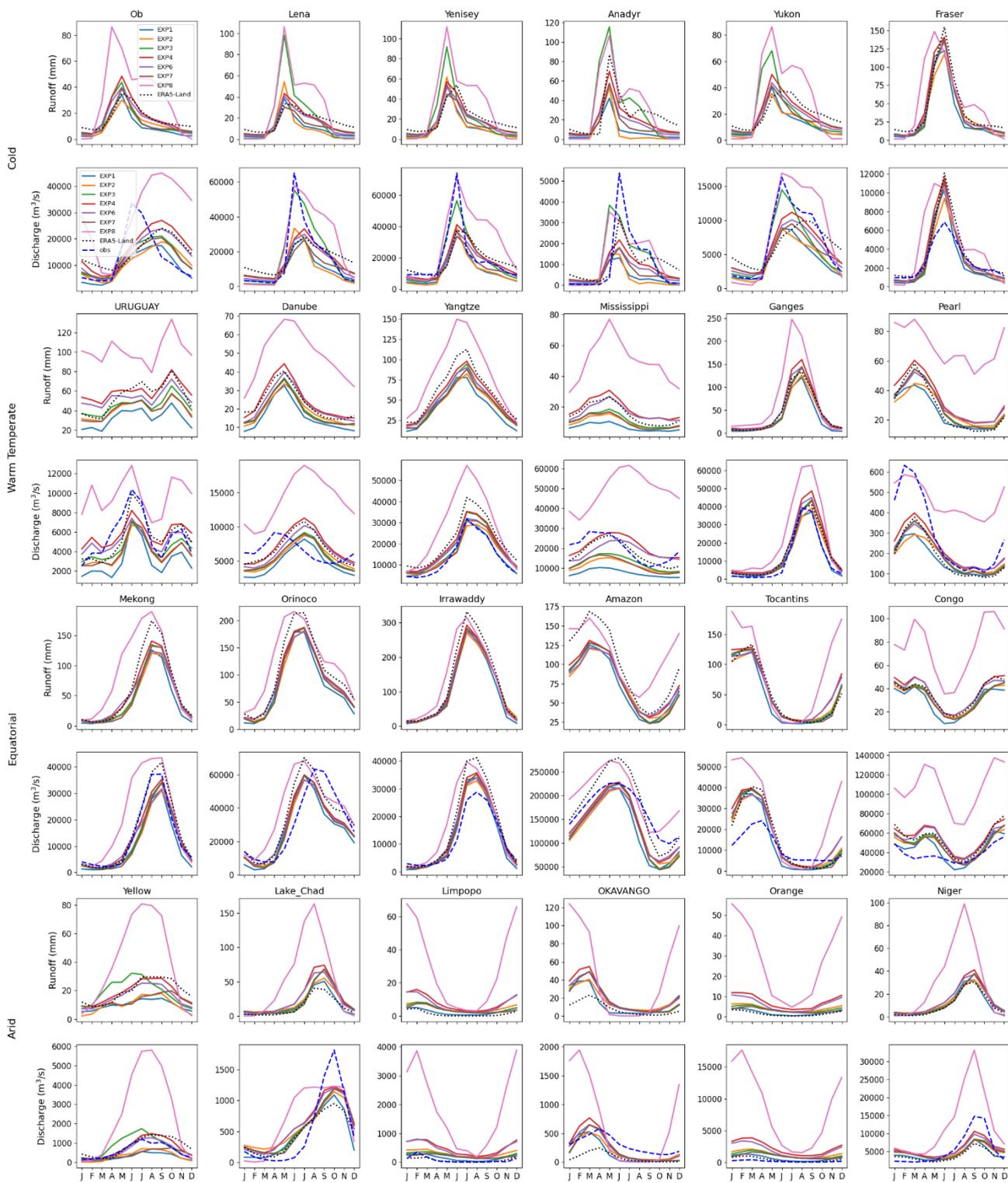
345 **Figure 3: Mean seasonal cycle of runoff (mm) and river discharge (m3/s) simulated by the different Noah-MP runoff schemes and CaMa-Flood, for 24 selected river basins representing four climate regions: top to bottom, rows are for cold, warm temperate, equatorial and arid regions. Discharge data includes simulated and observed values (obs) for the period 1985–2023. Observation years contributing to the monthly mean vary depending on their availability, with a minimum of 5 years per catchment.**

In equatorial regions, such as the Amazon and Orinoco basins, the seasonal cycle of runoff exhibits pronounced peaks during
350 wet seasons, directly translating into high discharge values. These peaks are expected due to intense rainfall and the vast drainage areas characteristic of these regions. The ability of the models to replicate these extreme events is essential for understanding and managing water resources in areas prone to significant seasonal variations.

In contrast, arid regions, including the Niger and Limpopo basins, display more subdued seasonal cycles of both runoff and discharge. This pattern reflects the typically low and irregular rainfall in these regions, leading to lower and less variable
355 runoff and, consequently, discharge. The consistency between runoff and discharge patterns in these regions illustrates the sensitivity of the models to regional climatic conditions.

Across many basins, while the runoff and discharge seasonal cycles are generally aligned, there is a noticeable delay between the peak runoff and the peak discharge, especially in large river basins such as the Amazon, where this lag can extend up to three months. This delay, ranging from a few days to several months depending on the basin physical
360 characteristics (e.g. basin size, basin shape, drainage density, river length, slop), is due to the natural routing lag within the river network, which involves the time it takes for water to travel through the system and the storage effects within the river channels.

However, another noticeable delay or lag in capturing the peak discharge by comparison to observed peaks, is highlighted as in the case of Ob and Danube river basins, which is not attributed to this natural routing lag. Instead, it is due to specific
365 limitations within the CaMa-Flood global river routing model. These limitations, particularly in certain model parameterizations and subsurface runoff schemes, hinder the model's ability to accurately predict the timing of maximum discharge. This temporal mismatch is critical for applications such as flood forecasting and water resource management. Supporting this, another river routing model, WRF-Hydro (Gochis et al., 2020), was tested using the same inputs (land surface model, schemes, forcing, resolution, and topography) for the Danube River basin. Unlike CaMa-Flood, WRF-Hydro
370 was able to capture the peak discharge timing accurately (not shown), confirming that the delay observed in CaMa-Flood simulations is due to the model's inherent limitations and thus not linked to the Noah-MP representation of runoff.

Both ERA5-Land and Noah-MP runoff-driven discharge successfully replicate the general patterns of the mean seasonal discharge cycle across most basins and climatic regions. This indicates a robust performance of the models in capturing the overall seasonal dynamics of river discharge. This capability is advantageous for conducting trend and frequency analysis
375 under climate change projections and scenarios, aiding in the development of water management strategies and climate actions. Additionally, these models can be used in conjunction with a set of climate models to build an ensemble model, effectively addressing the uncertainty in future projections.

Conversely, a significant positive bias is observed in EXP8, which tends to overestimate the seasonal cycle of discharge in the majority of the basins globally. This overestimation is evident when compared to ERA5-Land runoff-driven discharge as

380 well as to the other seven experimental setups. The consistent overestimation by EXP8 confirms the systematic issue within this particular runoff scheme. On the other side, EXP1 and EXP2 slightly underestimate discharge when compared to ERA5-Land in cold, warm temperate, and equatorial regions. However, these schemes slightly overestimate discharge in arid regions. This differential performance indicates region-specific biases in these runoff schemes that might be attributed to how they handle surface and subsurface runoff processes. The noticeable bias highlighted with these experiments reflects

385 clearly the translation of the aforementioned bias in runoff to a bias in discharge. This shows the significant influence that the selection of a particular runoff scheme can have on flow discharge.

Finally, we would highlight that all experimental setups and ERA5-Land sometimes tend to overestimate the discharge when compared to GRDC observations. This overestimation can be attributed to various factors, including basin regulation and human activities, observation accuracy, and forcing accuracy and resolution. These elements introduce complexities that

390 affect the ability of models to match observed discharge precisely.

3.3 Runoff Bias Propagation to Discharge Bias

After demonstrating the significant impact that the selection of a particular runoff scheme can have on flow discharge patterns, we now explore the relationship between runoff bias and discharge bias. According to the water balance equation, within a defined area over a specific period, the total inflows must equal the total outflows, plus any change in storage. When

395 considering periods longer than one year, the changes in water storage are generally assumed to be negligible ($\Delta S = 0$) (Oda et al., 2024). Under this assumption, the total runoff (including both surface and subsurface components) is nearly equal to the total discharge observed at the basin outlet. As a result, one would expect a strong correlation between runoff bias and discharge bias.

Figure 4 corroborates this expectation, illustrating the correlation between runoff and discharge biases when compared to

400 ERA5-Land runoff and simulated discharge across various climate zones and globally.
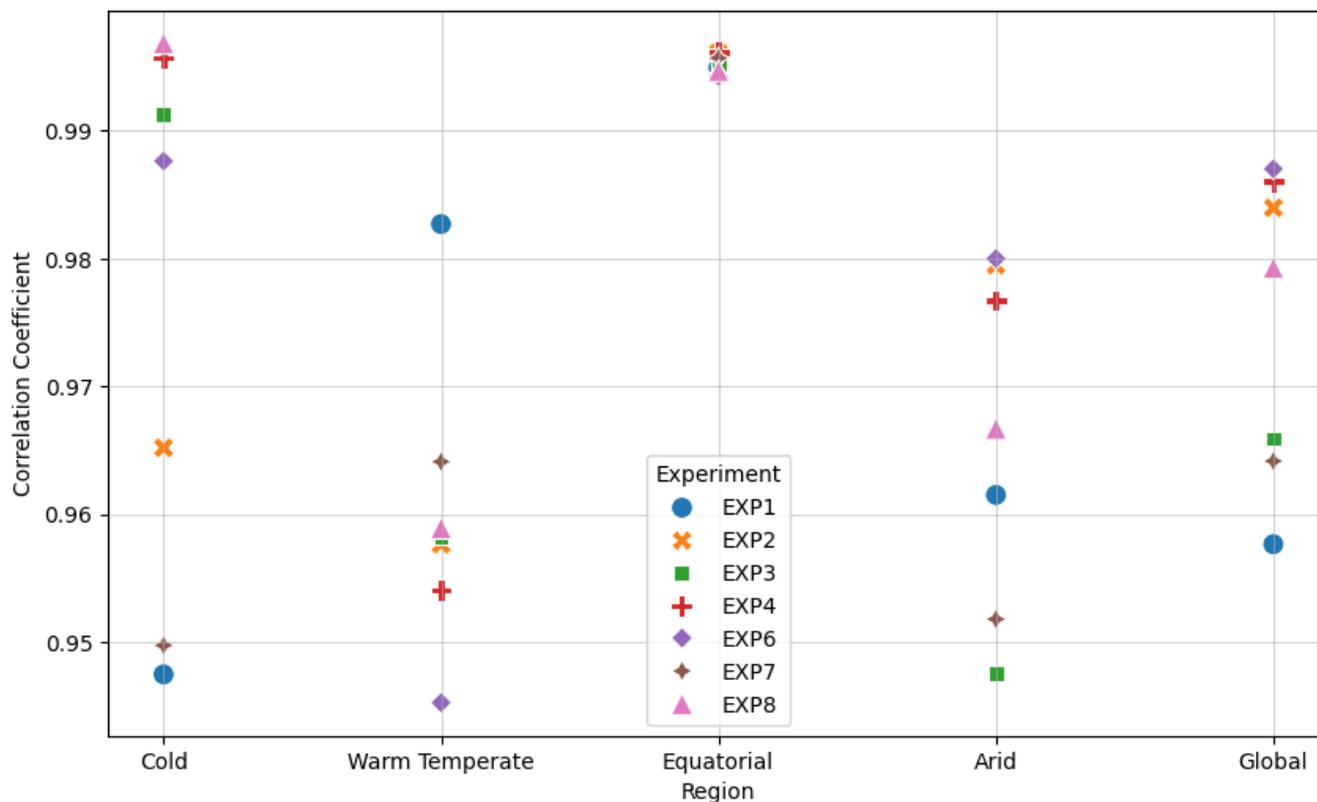
Figure 4: Scatter plots of Pearson correlation coefficients between runoff and discharge biases across climate regions and globally.

The correlation coefficients, ranging from 0.945 to 0.997, indicate an almost perfect agreement between the biases, highlighting the direct propagation of uncertainty from runoff to discharge estimation. This analytical finding aligns with the results of (https://doi.org/10.1029/2019GL083342), further emphasizing the critical influence that the choice of runoff scheme has on discharge bias.

3.4 Discharge Performance Metrics

Figure 5 and Table 1 present the performance statistical metrics, i.e. the Kling-Gupta Efficiency (KGE), Root Mean Square Error (RMSE), Mean Absolute Error (MAE), temporal correlation coefficient (R), and standard deviation (SD), of the different Noah-MP experiments across the four climate regions against the observational dataset GRDC (a detailed values regarding some of these metrics are provided for each river basin in the Tables S2, S3 and S4 in the Supplement). These metrics provide a comprehensive evaluation of each model's performance in capturing daily discharge, highlighting the strengths and limitations of each experimental setup in diverse climatic conditions.

Table 1: Performance metrics (KGE, RMSE (m³/s), MAE (m³/s)) of Noah-MP runoff models in terms of daily discharge across climate regions.

EXPs	Cold Regions			Warm Temperate Regions			Equatorial Regions			Arid Regions		
	KGE	RMSE	MAE	KGE	RMSE	MAE	KGE	RMSE	MAE	KGE	RMSE	MAE
EXP1	0.39	7578.3	3436.6	0.53	5716.5	2856.0	0.75	26212.9	13349.6	0.59	1241.9	549.2
EXP2	0.45	7274.0	3430.5	0.76	4693.2	2315.4	0.77	21529.6	11608.6	0.44	1375.5	810.6
EXP3	0.79	5900.8	2998.5	0.82	4647.9	2315.0	0.80	22992.3	11982.4	0.47	1344.0	759.8
EXP4	0.62	7290.8	3290.9	0.64	4922.2	2544.7	0.86	19576.9	10288.8	-0.11	1717.9	1171.4
EXP6	0.57	7247.5	3049.7	0.79	4532.0	2367.9	0.81	20675.1	11027.0	0.13	1564.0	1018.7
EXP7	0.45	7824.1	3342.8	0.78	4734.0	2369.2	0.80	23399.1	12171.5	0.55	1330.1	710.0
EXP8	0.12	11396.1	7089.8	-0.92	15244.6	8147.3	0.62	29853.7	19879.7	-4.14	6512.5	3836.1
ERA5-Land	0.55	8165.0	3964.2	0.87	3881.9	2003.5	0.84	18892.0	10555.2	0.52	1317.0	514.4
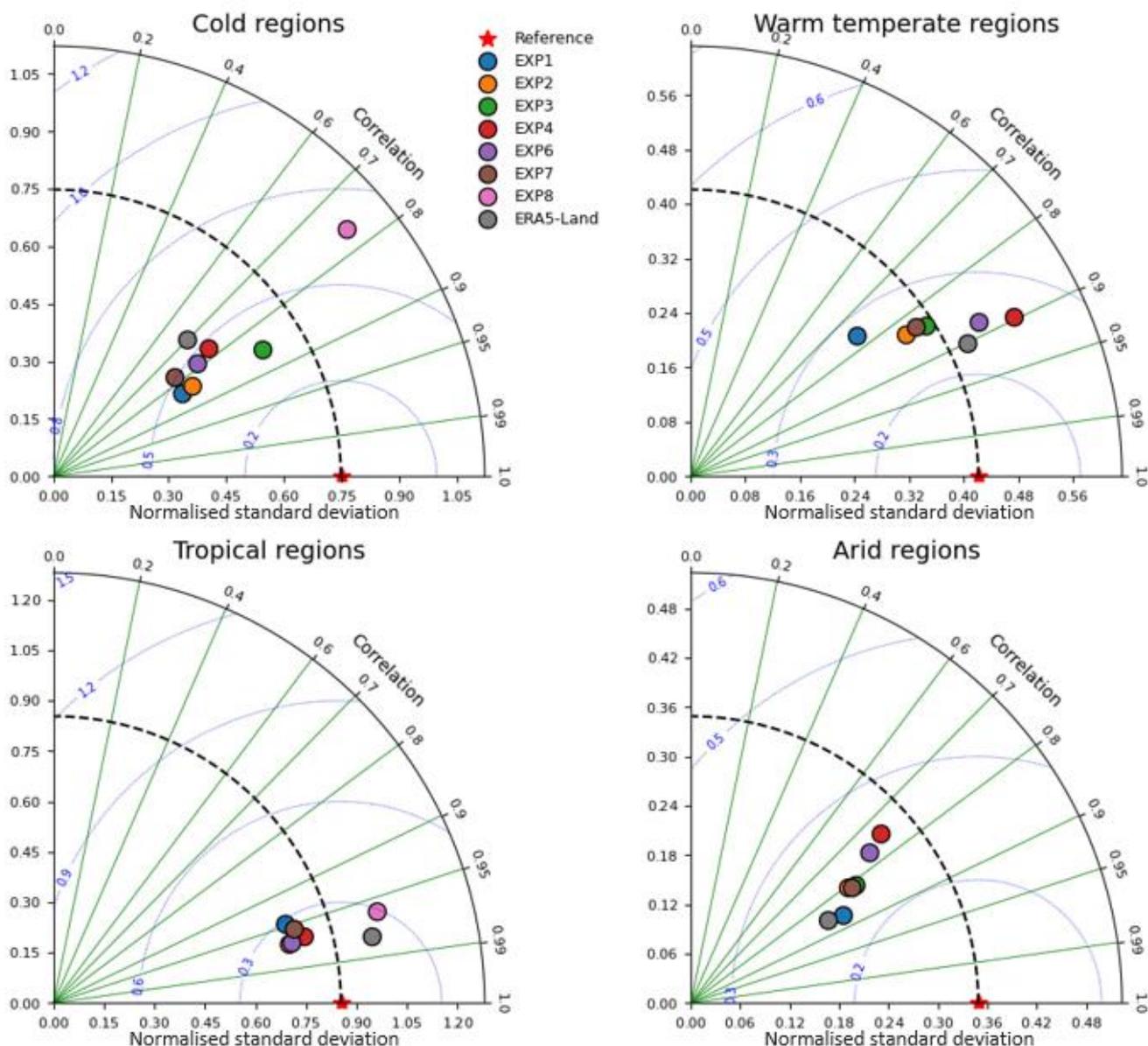
Figure 5: Taylor diagram showing the performances of Noah-MP runoff models in terms of daily discharge within four climate
420 regions.

Considering the Noah-MP performances in discharge simulation, in the cold regions, EXP3 exhibits the highest KGE (0.79)

and a high correlation coefficient (0.86), closely matching the observed standard deviation (SD). This model also has the

lowest RMSE (5900.8 m3/s) and MAE (2998.5 m3/s), indicating strong performance. EXP4 and EXP6, as well as ERA5-

Land, also perform well with KGEs of 0.62, 0.57 and 0.55, respectively, and reasonable error metrics. EXP1 and EXP2

425 perform moderately, with EXP1 showing a lower SD compared to observations, indicating an underestimation of discharge

variability. EXP8 performs poorly, with the lowest KGE (0.12) and the highest SD, RMSE, and MAE, indicating significant overestimation.

In warm temperate regions, ERA5-Land achieves the best performance with the highest KGE (0.87) and correlation coefficient (0.90), closely matching the observed SD and having the lowest RMSE (3881.9 m3/s) and MAE (2003.5 m3/s).

430   EXP3 also performs well with a KGE of 0.82 and low error metrics, followed by EXP6 and EXP7, both demonstrating strong performance. EXP2 shows balanced performance with a KGE of 0.76 and moderate error metrics. EXP1 performs moderately with a KGE of 0.53. EXP4, despite having a high correlation (0.90), shows overestimation with a higher SD and moderate errors. EXP8 again performs poorly with the lowest KGE (-0.92) and significantly high SD, RMSE, and MAE. Due to its exceptionally high standard deviation, which is 2.4 times higher than the observed SD, EXP8 is considered an

435   outlier in the Taylor diagram and does not appear in Fig. 5. For reference, its correlation coefficient is 0.88.

In equatorial regions, EXP4 and ERA5-Land show the highest performance with KGEs of 0.86 and 0.84, and a high correlation (0.97 and 0.98), respectively. These models closely align with the observed SD and exhibit the lowest RMSE (19576.9 m3/s and 18892.0 m3/s) and MAE (10288.8 m3/s and 10555.2 m3/s). EXP2, EXP3, EXP6 and EXP7 also perform well with KGEs of 0.77, 0.80, 0.81 and 0.80, respectively, and present moderate error metrics. EXP1 shows moderate

440   performance, while EXP8 performs poorly with the highest SD, RMSE, and MAE.

In arid regions, ERA5-Land again shows good performance with a KGE of 0.52 and a high correlation (0.85), closely matching the observed SD. EXP1 and EXP7 also perform reasonably well, with KGEs of 0.59 and 0.55, respectively. EXP2 and EXP3 show balanced performance with moderate KGEs. EXP6 shows a lower performance with a KGE of 0.13 and higher error metrics. EXP4 and EXP8 perform poorly, with EXP8 having the lowest KGE (-4.14) and the highest error

445   metrics, indicating significant overestimation. The high standard deviation of EXP8, which is almost three times higher than the observed SD, makes it an outlier in the Taylor diagram, hence it is not plotted. However, its correlation coefficient is 0.58.

Globally (Table 2), EXP4 shows the best performance with a KGE of 0.89, a high correlation (0.96), and reasonable error metrics. ERA5-Land also performs well with a high KGE (0.87) and moderate error metrics. EXP3 and EXP6 show strong

450   performance with KGEs of 0.82 and 0.84, respectively, and moderate error metrics. EXP2 and EXP1 demonstrate balanced performance with KGEs of 0.75 and 0.70, respectively. EXP7 performs moderately with a KGE of 0.78. EXP8, however, performs poorly with the lowest global KGE (0.31) and the highest SD, RMSE, and MAE, indicating significant overestimation.

455   **Table 2: Global Performance metrics of Noah-MP runoff models in terms of daily discharge.**

EXPs	Global				
	KGE	R	SD	RMSE	MAE
EXP1	0.70	0.95	27773.7	11628.8	4246.2
EXP2	0.75	0.97	27859.3	9791.5	3830.9

EXP3	0.82	0.96	28905.1	9995.4	3741.6
EXP4	0.89	0.96	30020.2	9200.4	3728.6
EXP6	0.84	0.97	28529.4	9476.5	3675.4
EXP7	0.78	0.96	28702.1	10558.2	3890.8
EXP8	0.31	0.95	41170.9	16359.7	8858.9
ERA5-Land	0.87	0.97	36919.6	9024.9	3677.4
Observations			33361.1		

Overall, ERA5-Land and Schaake approach (EXP3) consistently exhibit strong performance across different climate regions, closely aligning with observed data and demonstrating low error metrics. Other models like VIC and BATS (EXP 6 and 4) also perform well in specific regions, while Dynamic VIC (EXP8) consistently underperforms, showing substantial overestimation and high error metrics due to the strong overestimation in runoff.

The results presented are not surprising and are, in fact, reasonable given the characteristics of the different runoff schemes and the regions they are applied to. Schaake, an infiltration-excess runoff scheme (EXP3), performs the best in the northern mid-and-high latitude basins as stated in (Decharme, 2007), here corresponding to cold regions, i.e. areas dominated by snow and glaciers, which make the frozen soils less permeable. Additionally, the intensity of precipitation in these regions often exceeds the infiltration rate, thereby generating runoff through the infiltration-excess mechanism.

EXP3 also performs exceptionally well in warm temperate regions, which dominate the CONUS (Continental United States) domain. This superior performance likely justifies its status as the default option in WRF-Hydro/US National Water Model.

Schaake, along with BATS, VIC, and XAJ (i.e. respectively EXP3, 4, 6 and 7), shows strong performance in warm temperate and equatorial regions. This aligns with existing literature indicating that these schemes were developed and tested primarily in humid and sub-humid regions (Hao et al., 2015; Hou et al., 2023).

In arid regions, TOPMODEL with groundwater (EXP1) stands out, likely due to its incorporation of subsurface and groundwater processes, which enhance groundwater recharge and baseflow contributions—factors that are crucial in arid environments. The same reason could be behind its underestimation of runoff in humid and sub-humid regions. A study by (Gan et al., 2019) demonstrated that TOPMODEL with groundwater scheme produces the wettest soil and the greatest evapotranspiration across ten hydrologic regions of China, in contrast to the BATS scheme, which yields the driest soil and the smallest evapotranspiration.

ERA5-Land demonstrates very good performance at both global and regional scales, serving as an excellent reference dataset for runoff benchmarking.

The hydrological basins were also grouped based on dominant soil texture and land cover types to analyse the performance of the Noah-MP model. Additionally, the experiments' performances were correlated with the mean slope, as well as the basin size (Fig. S1 in the Supplement). No significant correlations were found overall, indicating that the Noah-MP model operates effectively regardless of land cover type, soil type, basin size, or topography. This lack of correlation suggests a robust versatility in the model's application, highlighting its capacity to provide reliable simulations across diverse

environmental conditions and varied landscape features. The findings reinforce the model's utility in different hydrological
485 contexts, supporting its use in global and regional hydrological studies without the need for extensive customisation based on
specific basin characteristics.

Although in general, except for Dynamic VIC, the experiments demonstrated good performance in capturing the overall
patterns of river discharge, there remains a considerable bias when applied to more detailed studies, particularly those
focusing on high-flow extremes. This bias affects the accuracy in capturing the magnitude, timing, and extent of these
490 events, indicating that further improvements are necessary. Each runoff scheme, with its unique conceptual framework,
involves a set of tuneable variables and parameters, such as: soil depth, maximum surface saturated fraction, saturated value
of soil moisture and others. Calibration of these variables and parameters, especially at finer resolutions, could significantly
enhance the results, making them more reliable for detailed hydrological studies.

We would like to underline that the obtained results and this study are biassed and constrained by the availability of high-
495 quality discharge observations within the considered study period. This limitation, along with the need for a consistent
evaluation period and the focus on less regulated basins, conditions the number of basins selected and their distribution
within each climate region.

4 Conclusions

This study evaluated the performance of seven different Noah-MP runoff schemes in discharge simulations, as simulated
500 using the CaMa-Flood River routing model. Using ERA5-Land runoff data as a benchmark for runoff evaluation and
streamflow observations for discharge evaluation across various climatic regions, key findings from the analysis reveal
significant differences in how each scheme handles runoff dynamics. These findings have important implications for
hydrological modelling and water resource management.

The progression from TOPMODEL-based schemes through Schaake, BATS and other saturation-excess schemes showed a
505 trend of decreasing bias magnitudes and improved performance in simulating runoff dynamics. TOPMODEL with
groundwater and TOPMODEL with an equilibrium water table significantly underestimated runoff in many regions,
particularly in the Northern Hemisphere, while runoff schemes like Schaake, BATS, VIC, and XAJ demonstrated
progressively better performance with relatively lower biases. Dynamic VIC consistently overestimated runoff across nearly
all regions.

510 Seasonal cycle analysis using CaMa-Flood driven by different Noah-MP runoff schemes highlighted considerable regional
and seasonal variability in discharge patterns. ERA5-Land runoff-driven discharge and several Noah-MP experiments
successfully replicated the general patterns of mean seasonal discharge cycles across diverse river basins. However,
Dynamic VIC showed a significant positive bias, indicating a tendency to overestimate discharge globally, due to the strong
runoff overestimation.

515   ERA5-Land and Schaake scheme consistently exhibited strong performance across different climate regions, closely aligning with observed data and demonstrating low error metrics. TOPMODEL, and Dynamic VIC showed higher error metrics, with more significant biases for Dynamic VIC, indicating the need for further refinement, although TOPMODEL with groundwater stands out as the most effective in arid regions.

The Noah-MP model demonstrated robust versatility, performing effectively regardless of land cover type, soil type, basin

520   size, or topography. This suggests that the model can provide reliable simulations across diverse environmental conditions without extensive customisation.

While the experiments generally captured the overall patterns of river discharge, significant biases remained, particularly in high-flow extremes. This underscores the need for ongoing calibration of tuneable variables and parameters, especially at finer resolutions, to enhance the accuracy and reliability of hydrological simulations.

525   In conclusion, this study highlights the strengths and limitations of different Noah-MP runoff schemes depending on the climatic region. The analysis underscores the significant impact that the selection of a particular runoff scheme can have on discharge patterns and bias, emphasizing the necessity for careful scheme selection based on specific hydrological contexts. Enhanced calibration and refinement efforts are essential for achieving more accurate hydrological predictions, which are vital for effective water resources management and climate adaptation strategies.

530   **Code and data availability**

GRDC   discharge   observations   can   be   obtained   from https://portal.grdc.bafg.de/applications/public.html?publicuser=PublicUser#dataDownload.

ERA5-Land data, provided by the European Centre for Medium-Range Weather Forecast (ECMWF), can be freely downloaded from the Copernicus Data Store (https://cds.climate.copernicus.eu/cdsapp#!/dataset/reanalysis-era5-

535   land?tab=overview).

Noah-MP and CaMa-flood models can be downloaded from https://github.com/NCAR/noahmp and https://github.com/global-hydrodynamics/CaMa-Flood_v4, respectively.

Enquiries about output data availability should be directed to the authors.

Author contribution

540   MH, GF, AA and CH: conceptualisation and methodology; MH: formal analysis, funding acquisition, investigation, visualisation and writing-original draft preparation; MH and AA: data collection, curation and simulations; GF and AA: supervision; GF, AA, CH and TL: validation and writing-review & editing. All authors have read and agreed to the published version of the paper.

Competing interests

545   The authors declare that they have no conflict of interest.

Acknowledgements

We would like to thank Dr. Stefan Hagemann and Dr. Stephen Birkinshaw (Hao et al., 2015) for providing us with some discharge observation data and Dr. Day Yamazaki for his valuable help in setting up the CaMa-flood model.

Financial support

550   This paper and related research have been conducted during and with the support of the Italian PhD course in Sustainable Development and Climate change (link: www.phd-sdc.it) at the University School for Advanced Studies IUSS and developed within the framework of the project "Dipartimento di Eccellenza 2023-2027"., with the financial support from the ICSC Italian Research Center on High-Performance Computing, Big Data and Quantum Computing and received funding from the European Union Next-GenerationEU (National Recovery and Resilience Plan-NRRP, Mission 4,
555   Component 2, Investment 1.4-D.D: 3138 16/12/2021, CN00000013).
This research has also been supported by the CIHEAM Prize for the Best MSc Thesis 2022.

References

Ball, J. T., Woodrow, I. E., and Berry, J. A.: A Model Predicting Stomatal Conductance and its Contribution to the Control of Photosynthesis under Different Environmental Conditions, in: Progress in Photosynthesis Research: Volume 4
560   Proceedings of the VIIth International Congress on Photosynthesis Providence, Rhode Island, USA, August 10–15, 1986, edited by: Biggins, J., Springer Netherlands, Dordrecht, 221–224, https://doi.org/10.1007/978-94-017-0519-6_48, 1987.

Balsamo, G., Beljaars, A., Scipal, K., Viterbo, P., van den Hurk, B., Hirschi, M., and Betts, A. K.: A Revised Hydrology for the ECMWF Model: Verification from Field Site to Terrestrial Water Storage and Impact in the Integrated Forecast System,
565   J Hydrometeorol, 10, 623–643, https://doi.org/10.1175/2008JHM1068.1, 2009.

Bates, P. D., Horritt, M. S., and Fewtrell, T. J.: A simple inertial formulation of the shallow water equations for efficient two-dimensional flood inundation modelling, J Hydrol (Amst), 387, 33–45, https://doi.org/10.1016/j.jhydrol.2010.03.027, 2010.
570

Bonan, G. B.: Land surface model (LSM version 1.0) for ecological, hydrological, and atmospheric studies: Technical description and users guide. Technical note, National Center for Atmospheric Research, Boulder, CO (United States …, https://doi.org/10.5065/D6DF6P5X, 1996.

575 Chang, M., Liao, W., Wang, X., Zhang, Q., Chen, W., Wu, Z., and Hu, Z.: An optimal ensemble of the Noah-MP land surface model for simulating surface heat fluxes over a typical subtropical forest in South China, Agric For Meteorol, 281, 107815, https://doi.org/10.1016/j.agrformet.2019.107815, 2020.

Chen, F. and Dudhia, J.: Coupling an Advanced Land Surface–Hydrology Model with the Penn State–NCAR MM5
580 Modeling System. Part I: Model Implementation and Sensitivity, Mon Weather Rev, 129, 569–585, https://doi.org/10.1175/1520-0493(2001)129<0569:CAALSH>2.0.CO;2, 2001.

Chen, F., Mitchell, K., Schaake, J., Xue, Y., Pan, H.-L., Koren, V., Duan, Q. Y., Ek, M., and Betts, A.: Modeling of land surface evaporation by four schemes and comparison with FIFE observations, Journal of Geophysical Research:
585 Atmospheres, 101, 7251–7268, https://doi.org/10.1029/95JD02165, 1996.

Chen, F., Janjić, Z., and Mitchell, K.: Impact of Atmospheric Surface-layer Parameterizations in the new Land-surface Scheme of the NCEP Mesoscale Eta Model, Boundary Layer Meteorol, 85, 391–421, https://doi.org/10.1023/A:1000531001463, 1997.
590
Clark, M. P., Fan, Y., Lawrence, D. M., Adam, J. C., Bolster, D., Gochis, D. J., Hooper, R. P., Kumar, M., Leung, L. R., Mackay, D. S., Maxwell, R. M., Shen, C., Swenson, S. C., and Zeng, X.: Improving the representation of hydrologic processes in Earth System Models, Water Resour Res, 51, 5929–5956, https://doi.org/10.1002/2015WR017096, 2015.

595 David, C. H., Hobbs, J. M., Turmon, M. J., Emery, C. M., Reager, J. T., and Famiglietti, J. S.: Analytical Propagation of Runoff Uncertainty Into Discharge Uncertainty Through a Large River Network, Geophys Res Lett, 46, 8102–8113, https://doi.org/10.1029/2019GL083342, 2019.

Decharme, B.: Influence of runoff parameterization on continental hydrology: Comparison between the Noah and the ISBA
600 land surface models, Journal of Geophysical Research: Atmospheres, 112, https://doi.org/10.1029/2007JD008463, 2007.

Dickinson, R. E.: Land Surface Processes and Climate—Surface Albedos and Energy Balance, in: Advances in Geophysics, vol. 25, edited by: Saltzman, B., Elsevier, 305–353, https://doi.org/10.1016/S0065-2687(08)60176-4, 1983.

605   Dickinson, R. E., Shaikh, M., Bryant, R., and Graumlich, L.: Interactive Canopies for a Climate Model, J Clim, 11, 2823–2836, https://doi.org/10.1175/1520-0442(1998)011<2823:ICFACM>2.0.CO;2, 1998.

DÜMENIL, L. and TODINI, E.: Chapter 9 - A rainfall–runoff scheme for use in the Hamburg climate model, in: Advances in Theoretical Hydrology, edited by: O'Kane, J. P., Elsevier, Amsterdam, 129–157, https://doi.org/10.1016/B978-0-444-610   89831-9.50016-8, 1992.

Ek, M. B., Mitchell, K. E., Lin, Y., Rogers, E., Grunmann, P., Koren, V., Gayno, G., and Tarpley, J. D.: Implementation of Noah land surface model advances in the National Centers for Environmental Prediction operational mesoscale Eta model, Journal of Geophysical Research: Atmospheres, 108, https://doi.org/10.1029/2002JD003296, 2003.

615

Fan, Y., Miguez-Macho, G., Weaver, C. P., Walko, R., and Robock, A.: Incorporating water table dynamics in climate modeling: 1. Water table observations and equilibrium water table simulations, Journal of Geophysical Research: Atmospheres, 112, https://doi.org/10.1029/2006JD008111, 2007.

620   Fang, Y.-H., Zhang, X., Corbari, C., Mancini, M., Niu, G.-Y., and Zeng, W.: Improving the Xin'anjiang hydrological model based on mass–energy balance, Hydrol Earth Syst Sci, 21, 3359–3375, https://doi.org/10.5194/hess-21-3359-2017, 2017.

Gan, Y., Liang, X.-Z., Duan, Q., Chen, F., Li, J., and Zhang, Y.: Assessment and Reduction of the Physical Parameterization Uncertainty for Noah-MP Land Surface Model, Water Resour Res, 55, 5518–5538, https://doi.org/10.1029/2019WR024814, 625   2019.

Gochis, D. J., Barlage, M., Cabell, R., Casali, M., Dugger, A., Fitzgerald, K., Karsten, L., Mcallister, M., McCreight, J., Rafieeinasab, A., Read, L., Sampson, K., Yates, D., and Zhang, Y.: The WRF-Hydro Modeling System Technical Description, (Version 5.1.1), NCAR Technical Note. 108 pages, 2020.

630

Gupta, H. V, Kling, H., Yilmaz, K. K., and Martinez, G. F.: Decomposition of the mean squared error and NSE performance criteria: Implications for improving hydrological modelling, J Hydrol (Amst), 377, 80–91, https://doi.org/10.1016/j.jhydrol.2009.08.003, 2009.

635   Hagemann, S. and Stacke, T.: Complementing ERA5 and E-OBS with high-resolution river discharge over Europe, Oceanologia, 65, 230–248, https://doi.org/10.1016/j.oceano.2022.07.003, 2023.

Hao, F., Sun, M., Geng, X., Huang, W., and Ouyang, W.: Coupling the Xinanjiang model with geomorphologic instantaneous unit hydrograph for flood forecasting in northeast China, International Soil and Water Conservation Research, 640 3, 66–76, https://doi.org/10.1016/j.iswcr.2015.03.004, 2015.

He, C., Valayamkunnath, P., Barlage, M., Chen, F., Gochis, D., Cabell, R., Schneider, T., Rasmussen, R., Niu, G.-Y., Yang, Z.-L., Niyogi, D., and Ek, M.: Modernizing the open-source community Noah with multi-parameterization options (Noah-MP) land surface model (version 5.0) with enhanced modularity, interoperability, and applicability, Geosci Model Dev, 16, 645 5131–5151, https://doi.org/10.5194/gmd-16-5131-2023, 2023a.

He, C., Valayamkunnath, P., Barlage, M., Gochis, D., Cabell, R., Schneider, T., Rasmussen, R., Niu, G.-Y., Yang, Z.-L., Niyogi, D., and Ek, M.: The Community Noah-MP Land Surface Modeling System Technical Description Version 5.0, https://doi.org/10.5065/ew8g-yr95, 2023b.

650

Heber Green, W. and Ampt, G. A.: Studies on Soil Phyics., J Agric Sci, 4, 1–24, https://doi.org/DOI: 10.1017/S0021859600001441, 1911.

Hirabayashi, Y., Mahendran, R., Koirala, S., Konoshima, L., Yamazaki, D., Watanabe, S., Kim, H., and Kanae, S.: Global 655 flood risk under climate change, Nat Clim Chang, 3, 816–821, https://doi.org/10.1038/nclimate1911, 2013.

Hou, Y., Guo, H., Yang, Y., and Liu, W.: Global Evaluation of Runoff Simulation From Climate, Hydrological and Land Surface Models, Water Resour Res, 59, e2021WR031817, https://doi.org/10.1029/2021WR031817, 2023.

660 Jayawardena, A. W. and Zhou, M. C.: A modified spatial soil moisture storage capacity distribution curve for the Xinanjiang model, J Hydrol (Amst), 227, 93–113, https://doi.org/10.1016/S0022-1694(99)00173-0, 2000.

Kottek, M., Grieser, J., Beck, C., Rudolf, B., and Rubel, F.: World Map of the Köppen?Geiger climate classification updated, Meteorologische Zeitschrift, 15, 259–263, https://doi.org/10.1127/0941?2948/2006/0130, 2006.

665

Li, J., Chen, F., Lu, X., Gong, W., Zhang, G., and Gan, Y.: Quantifying Contributions of Uncertainties in Physical Parameterization Schemes and Model Parameters to Overall Errors in Noah-MP Dynamic Vegetation Modeling, J Adv Model Earth Syst, 12, e2019MS001914, https://doi.org/10.1029/2019MS001914, 2020a.

670 Li, J., Chen, F., Lu, X., Gong, W., Zhang, G., and Gan, Y.: Quantifying Contributions of Uncertainties in Physical Parameterization Schemes and Model Parameters to Overall Errors in Noah-MP Dynamic Vegetation Modeling, J Adv Model Earth Syst, 12, e2019MS001914, https://doi.org/10.1029/2019MS001914, 2020b.

Li, J., Miao, C., Zhang, G., Fang, Y.-H., Shangguan, W., and Niu, G.-Y.: Global Evaluation of the Noah-MP Land Surface
675 Model and Suggestions for Selecting Parameterization Schemes, Journal of Geophysical Research: Atmospheres, 127, e2021JD035753, https://doi.org/10.1029/2021JD035753, 2022.

Liang, J., Yang, Z., and Lin, P.: Systematic Hydrological Evaluation of the Noah-MP Land Surface Model over China, Adv Atmos Sci, 36, 1171–1187, https://doi.org/10.1007/s00376-019-9016-y, 2019.
680
Liang, X. and Xie, Z.: A new surface runoff parameterization with subgrid-scale soil heterogeneity for land surface models, Adv Water Resour, 24, 1173–1193, https://doi.org/10.1016/S0309-1708(01)00032-X, 2001.

Liang, X. and Xie, Z.: Important factors in land–atmosphere interactions: surface runoff generations and interactions
685 between surface and groundwater, Glob Planet Change, 38, 101–114, https://doi.org/10.1016/S0921-8181(03)00012-2, 2003.

Liang, X., Lettenmaier, D. P., Wood, E. F., and Burges, S. J.: A simple hydrologically based model of land surface water and energy fluxes for general circulation models, Journal of Geophysical Research: Atmospheres, 99, 14415–14428, https://doi.org/10.1029/94JD00483, 1994.
690
Liu, L., Yi, Y., Jiang, H., Ran, Y., and Chen, D.: ERA5-Land overestimates runoff coefficient but underestimates runoff recession rate in the central Tibetan permafrost region, J Hydrol Reg Stud, 53, 101792, https://doi.org/10.1016/j.ejrh.2024.101792, 2024.

695 Miguez-Macho, G., Fan, Y., Weaver, C. P., Walko, R., and Robock, A.: Incorporating water table dynamics in climate modeling: 2. Formulation, validation, and soil moisture simulation, Journal of Geophysical Research: Atmospheres, 112, https://doi.org/10.1029/2006JD008112, 2007.

Miller, D. A. and White, R. A.: A Conterminous United States Multilayer Soil Characteristics Dataset for Regional Climate
700 and Hydrology Modeling, Earth Interact, 2, 1–26, https://doi.org/10.1175/1087-3562(1998)002<0001:ACUSMS>2.3.CO;2, 1998.

Monin, A. S. and Obukhov, A. M.: Basic laws of turbulent mixing in the atmosphere near the ground. vol. 24, Tr Akad Nauk SSSR Geofiz Inst, 163–187, 1954.

705

Muñoz-Sabater, J., Dutra, E., Agusti-Panareda, A., Albergel, C., Arduini, G., Balsamo, G., Boussetta, S., Choulga, M., Harrigan, S., Hersbach, H., Martens, B., Miralles, D. G., Piles, M., Rodriguez-Fernández, N. J., Zsoter, E., Buontempo, C., and Thépaut, J.-N.: ERA5-Land: a state-of-the-art global reanalysis dataset for land applications, Earth Syst Sci Data, 13, 4349–4383, https://doi.org/10.5194/essd-13-4349-2021, 2021.

710

Nguyen, A. D., Le Nguyen, P., Vu, V. H., Pham, Q. V., Nguyen, V. H., Nguyen, M. H., Nguyen, T. H., and Nguyen, K.: Accurate discharge and water level forecasting using ensemble learning with genetic algorithm and singular spectrum analysis-based denoising, Sci Rep, 12, 19870, https://doi.org/10.1038/s41598-022-22057-8, 2022.

715 Niu, G. Y. and Yang, Z.: The Community Noah Land Surface Model (LSM) with Multi-Physics Options, User's Guide, Center for Integrated Earth System Science, The University of Texas at Austin: Austin, TX, USA, 2011.

Niu, G.-Y. and Yang, Z.-L.: Effects of Frozen Soil on Snowmelt Runoff and Soil Water Storage at a Continental Scale, J Hydrometeorol, 7, 937–952, https://doi.org/10.1175/JHM538.1, 2006.

720

Niu, G.-Y., Yang, Z.-L., Dickinson, R. E., and Gulden, L. E.: A simple TOPMODEL-based runoff parameterization (SIMTOP) for use in global climate models, Journal of Geophysical Research: Atmospheres, 110, https://doi.org/10.1029/2005JD006111, 2005.

725 Niu, G.-Y., Yang, Z.-L., Dickinson, R. E., Gulden, L. E., and Su, H.: Development of a simple groundwater model for use in climate models and evaluation with Gravity Recovery and Climate Experiment data, Journal of Geophysical Research: Atmospheres, 112, https://doi.org/10.1029/2006JD007522, 2007.

Niu, G.-Y., Yang, Z.-L., Mitchell, K. E., Chen, F., Ek, M. B., Barlage, M., Kumar, A., Manning, K., Niyogi, D., Rosero, E., 730 Tewari, M., and Xia, Y.: The community Noah land surface model with multiparameterization options (Noah-MP): 1. Model description and evaluation with local-scale measurements, Journal of Geophysical Research: Atmospheres, 116, https://doi.org/10.1029/2010JD015139, 2011.

Oda, T., Iwasaki, K., Egusa, T., Kubota, T., Iwagami, S., Iida, S., Momiyama, H., and Shimizu, T.: Scale-Dependent Inter-735 Catchment Groundwater Flow in Forested Catchments: Analysis of Multi-Catchment Water Balance Observations in Japan, Water Resour Res, 60, e2024WR037161, https://doi.org/10.1029/2024WR037161, 2024.

Philip, J. R.: The infiltration joining problem, Water Resour Res, 23, 2239–2245, https://doi.org/10.1029/WR023i012p02239, 1987.

740

Ren-Jun, Z.: The Xinanjiang model applied in China, J Hydrol (Amst), 135, 371–381, https://doi.org/10.1016/0022-1694(92)90096-E, 1992.

Rummler, T., Wagner, A., Arnault, J., and Kunstmann, H.: Lateral terrestrial water fluxes in the LSM of WRF-Hydro:

745 Benefits of a 2D groundwater representation, Hydrol Process, 36, e14510, https://doi.org/10.1002/hyp.14510, 2022.

Sakaguchi, K. and Zeng, X.: Effects of soil wetness, plant litter, and under-canopy atmospheric stability on ground evaporation in the Community Land Model (CLM3.5), Journal of Geophysical Research: Atmospheres, 114, https://doi.org/10.1029/2008JD010834, 2009.

750

Schaake, J. C., Koren, V. I., Duan, Q.-Y., Mitchell, K., and Chen, F.: Simple water balance model for estimating runoff at different spatial and temporal scales, Journal of Geophysical Research: Atmospheres, 101, 7461–7475, /https://doi.org/10.1029/95JD02892, 1996.

755 SELLERS, P. J.: Canopy reflectance, photosynthesis and transpiration, Int J Remote Sens, 6, 1335–1372, https://doi.org/10.1080/01431168508948283, 1985.

Sheng, M., Lei, H., Jiao, Y., and Yang, D.: Evaluation of the Runoff and River Routing Schemes in the Community Land Model of the Yellow River Basin, J Adv Model Earth Syst, 9, 2993–3018, https://doi.org/10.1002/2017MS001026, 2017.

760

Smith, R. E. and Parlange, J.-Y.: A parameter-efficient hydrologic infiltration model, Water Resour Res, 14, 533–538, https://doi.org/10.1029/WR014i003p00533, 1978.

Stephens, G. L., Slingo, J. M., Rignot, E., Reager, J. T., Hakuba, M. Z., Durack, P. J., Worden, J., and Rocca, R.: Earth's

765 water reservoirs in a changing climate, Proceedings of the Royal Society A: Mathematical, Physical and Engineering Sciences, 476, 20190458, https://doi.org/10.1098/rspa.2019.0458, 2020.

Taylor, K. E.: Summarizing multiple aspects of model performance in a single diagram, Journal of Geophysical Research: Atmospheres, 106, 7183–7192, https://doi.org/10.1029/2000JD900719, 2001.

770

Verseghy, D. L.: Class—A Canadian land surface scheme for GCMS. I. Soil model, International Journal of Climatology, 11, 111–133, /https://doi.org/10.1002/joc.3370110202, 1991.

Wipfler, E. L., Metselaar, K., van Dam, J. C., Feddes, R. A., van Meijgaard, E., van Ulft, L. H., van den Hurk, B., Zwart, S.

775 J., and Bastiaanssen, W. G. M.: Seasonal evaluation of the land surface scheme HTESSEL against remote sensing derived energy fluxes of the Transdanubian region in Hungary, Hydrol Earth Syst Sci, 15, 1257–1271, https://doi.org/10.5194/hess-15-1257-2011, 2011.

Yamazaki, D., Kanae, S., Kim, H., and Oki, T.: A physically based description of floodplain inundation dynamics in a global

780 river routing model, Water Resour Res, 47, https://doi.org/10.1029/2010WR009726, 2011.

Yamazaki, D., de Almeida, G. A. M., and Bates, P. D.: Improving computational efficiency in global river models by implementing the local inertial flow equation and a vector-based river network map, Water Resour Res, 49, 7221–7235, https://doi.org/10.1002/wrcr.20552, 2013.

785

Yamazaki, D., Sato, T., Kanae, S., Hirabayashi, Y., and Bates, P. D.: Regional flood dynamics in a bifurcating mega delta simulated in a global river model, Geophys Res Lett, 41, 3127–3135, https://doi.org/10.1002/2014GL059744, 2014.

Yang, W.-Y., Li, D., Sun, T., and Ni, G.-H.: Saturation-excess and infiltration-excess runoff on green roofs, Ecol Eng, 74,

790 327–336, https://doi.org/10.1016/j.ecoleng.2014.10.023, 2015.

Yang, Z.-L. and Dickinson, R. E.: Description of the Biosphere-Atmosphere Transfer Scheme (BATS) for the Soil Moisture Workshop and evaluation of its performance, Glob Planet Change, 13, 117–134, https://doi.org/10.1016/0921-8181(95)00041-0, 1996.

795

Yang, Z.-L., Niu, G.-Y., Mitchell, K. E., Chen, F., Ek, M. B., Barlage, M., Longuevergne, L., Manning, K., Niyogi, D., Tewari, M., and Xia, Y.: The community Noah land surface model with multiparameterization options (Noah-MP): 2. Evaluation over global river basins, Journal of Geophysical Research: Atmospheres, 116, https://doi.org/10.1029/2010JD015140, 2011.

800

Zhang, G., Chen, F., and Gan, Y.: Assessing uncertainties in the Noah-MP ensemble simulations of a cropland site during the Tibet Joint International Cooperation program field campaign, Journal of Geophysical Research: Atmospheres, 121, 9576–9596, https://doi.org/10.1002/2016JD024928, 2016a.

805   Zhang, G., Chen, F., and Gan, Y.: Assessing uncertainties in the Noah-MP ensemble simulations of a cropland site during the Tibet Joint International Cooperation program field campaign, Journal of Geophysical Research: Atmospheres, 121, 9576–9596, https://doi.org/10.1002/2016JD024928, 2016b.

Zhang, G., Li, J., Zhou, G., Cai, X., Gao, W., Peng, X., and Chen, Y.: Effects of Mosaic Representation of Land Use/Land
810   Cover on Skin Temperature and Energy Fluxes in Noah-MP Land Surface Model Over China, Journal of Geophysical Research: Atmospheres, 126, e2021JD034542, https://doi.org/10.1029/2021JD034542, 2021a.

Zhang, Q., Wang, B.-D., He, B., Peng, Y., and Ren, M.-L.: Singular Spectrum Analysis and ARIMA Hybrid Model for Annual Runoff Forecasting, Water Resources Management, 25, 2683–2703, https://doi.org/10.1007/s11269-011-9833-y,
815   2011.

Zhang, X., Chen, L., Ma, Z., and Gao, Y.: Assessment of surface exchange coefficients in the Noah-MP land surface model for different land-cover types in China, International Journal of Climatology, 41, 2638–2659, https://doi.org/10.1002/joc.6981, 2021b.

820

Zheng, D., Van Der Velde, R., Su, Z., Wen, J., and Wang, X.: Assessment of Noah land surface model with various runoff parameterizations over a Tibetan river, Journal of Geophysical Research: Atmospheres, 122, 1488–1504, https://doi.org/10.1002/2016JD025572, 2017.

825   Zheng, H., Yang, Z.-L., Lin, P., Wei, J., Wu, W.-Y., Li, L., Zhao, L., and Wang, S.: On the Sensitivity of the Precipitation Partitioning Into Evapotranspiration and Runoff in Land Surface Parameterizations, Water Resour Res, 55, 95–111, https://doi.org/10.1029/2017WR022236, 2019.

Zipper, S. C., Motew, M., Booth, E. G., Chen, X., Qiu, J., Kucharik, C. J., Carpenter, S. R., and Loheide II, S. P.:
830   Continuous separation of land use and climate effects on the past and future water balance, J Hydrol (Amst), 565, 106–122, https://doi.org/10.1016/j.jhydrol.2018.08.022, 2018.